

Circuit Design and Experimental Investigations for a Predator-Prey Model

Afef Ben Saad, Ali Hmidet and
Olfa Boubaker

National Institute of Applied
Sciences and Technology, INSAT,
Centre Urbain Nord BP. 676,
1080 Tunis Cedex, Tunisia.

E-mail: afef.ben.saad88@gmail.com,
hmidetali@yahoo.fr,
olfa.boubaker@insat.rnu.tn.

This article was edited by Tariqu
Islam.

Received for publication January 12,
2018.

Abstract

In recent years, dynamical relationship between species in ecology has been intensively investigated and will continue to be one of the most significant themes. The dynamics of predator-prey's systems are at the heart of these studies. Such models are generally depicted by nonlinear polynomials and exhibit many complex nonlinear phenomena. In this paper, not only a prey-predator model displaying richer dynamical behaviors is analyzed but also its electronic circuit is also designed via the MultiSIM software proving the very good agreement between biological theory considerations and electronic experiments.

Keywords

Circuit design, MultiSIM, experiments, predator-prey model.

Ecology is the study of interactions among organisms and their environment. There are many useful applications of ecology as natural resource management and city planning (Laktionov et al., 2017; Teay et al., 2017; Umar et al., 2017; Visconti et al., 2017). However, ecology is also concerned by understanding and analyzing the dynamical behavior of populations in ecosystem in order to predict their undesired dynamics (Feng et al., 2017; Zhang et al., 2017b). On the other hand, understanding population dynamics are leading nowadays to many interesting optimization algorithms such as *Particle Swarm* algorithms (Mehdi and Boubaker, 2011, 2016;), Ant Colony algorithms (Pang et al., 2017; Yongwang et al., 2017) and Prey-predator algorithms (Sidhu and Dhillon, 2017; Zhang and Duan, 2017).

It is obvious that it is not at all evident to construct a mathematical model that will fit entirely any natural population interactions. In the literature, several models for predator-prey's systems have been already proposed and analyzed incorporating some specific effects (Bürger et al., 2017; Elettrey et al., 2017; Li et al., 2017a, 2017b; Liu et al., 2017, 2018; Liu and Dai, 2018; Wang and Yuan et al., 2018; Zhang et al., 2017a). The first proposed one was the Lotka Volterra predator-prey model (Volterra, 1928). However, to the best of our knowledge, there is no research work that

attempt to reproduce the complex dynamics of such systems using an equivalent electrical circuit. While, certain biological systems such as biological tissue and biological neural network are modeled by electrical circuit (Le Masson et al., 1999; Gómez et al., 2012). As such predator-prey systems exhibit complex dynamics as chaotic behaviors (Luo et al., 2016), such circuits can be adopted in the future in communication for encryption tasks (Lassoued and Boubaker, 2016; Lassoued and Boubaker, 2017; Kengne et al., 2017).

In this paper, the predator-prey system, already analyzed in Ben Saad and Boubaker (2015, 2017), and incorporating nonlinear polynomials in its complex model is considered for the weak Allee Effect case study. The objective is to design a suitable electronic circuit permitting to understand and conceptualize many aspects of ecological experimentation and theory by using only simple analog electronic components. It is clear that proving a good agreement between biological theory and electronic experiments is not evident due to the imperfections and uncertainties related to electronic components. Despite, these undesirable effects, the main nonlinearities of the biological model will be validated by means of experimental data. The circuit related to the prey-predator model will be then designed and simulated using the MultiSIM software.

This work is arranged as follows: Sections “PREDATOR–PREY MATHEMATICAL MODEL” and “WEAK ALLEE EFFECT CASE STUDY ANALYSIS” recall the nonlinear model as well as its basic dynamics. Then, numerical simulation of the global dynamic behavior of the system is presented in Section “NUMERICAL SIMULATIONS VIA MATCONT SOFTWARE”. In Section “EXPERIMENTAL VALIDATION OF MAIN NON-LINEARITIES”, the circuit design, simulation results via the MultiSIM software as well as the experimental data of the main nonlinearities of the predator–prey model are investigated. In Section “CIRCUIT DESIGN VIA MULTISIM SOFTWARE”, the circuit design of the whole complex model is finally proposed and a good agreement between simulation results via MATCONT and MultiSIM softwares are shown. Finally, an experimental implementation is illustrated in section “EXPERIMENTAL IMPLEMENTATION OF THE PREDATOR–PREY MODEL”.

Predator–Prey mathematical model

Consider the predator–prey model with Allee Effect described by Ben Saad and Boubaker, (2015, 2017):

$$\begin{cases} \frac{dx_1}{dt} = x_1(x_1 - \ell)(k - x_1) - x_1x_2, \\ \frac{dx_2}{dt} = e(x_1 - m)x_2, \end{cases} \quad (1)$$

where x_1 is the size of the prey population and x_2 the size of the predator population, ℓ is the Allee Effect threshold, k is the carrying capacity, e is the feeding efficiency of Lotka–Volterra model and m is the predator mortality rate. Let consider also the biologically meaningful conditions $x_1 \geq 0$ and $x_2 \geq 0$.

Two case studies for the Allee effect ℓ can be considered (Dhooge et al., 2008):

- The Strong Allee effect when $\ell \in [0, 1]$,
- The Weak Allee effect when $\ell \in [-1, 0]$.

In the following, only the Weak Allee effect case study will be considered and the parameters k , e , and m are taken as $k=e=1$ and $m \in [0, 1]$.

Weak alle effect case study analysis

For $k=e=1$, $\ell \in [-1, 0]$ and $m \in [0, 1]$, the system (1) admits three equilibriums $E_i (i=1, \dots, 3)$:

1. The zero equilibrium $E_0 = (0, 0)$,
2. The two non-isolated equilibriums $E_1 = (\ell, 0)$,
3. The equilibrium $E_2 = (m, (m - \ell)(1 - m))$.

For $i=1, \dots, 3$, the corresponding Jacobian matrix J_i and eigenvalues $(\lambda_{1i}, \lambda_{2i})$ are given by

$$J_0 = \begin{pmatrix} -\ell & 0 \\ 0 & -m \end{pmatrix} \quad \text{and} \quad \begin{cases} \lambda_{10} = -\ell \\ \lambda_{20} = -m \end{cases} \quad (2)$$

$$J_1 = \begin{pmatrix} (\ell - 1) & -1 \\ 0 & (1 - m) \end{pmatrix} \quad \text{and} \quad \begin{cases} \lambda_{11} = \ell - 1 \\ \lambda_{21} = 1 - m \end{cases} \quad (3)$$

$$J_3 = \begin{pmatrix} (-2m^2 + m(\ell + 1)) & -m \\ (m - \ell)(1 - m) & 0 \end{pmatrix} \quad \text{and} \quad \begin{cases} \lambda_{12} = \frac{\text{tr}(J_3) + i\sqrt{\Delta}}{2} \\ \lambda_{22} = \frac{\text{tr}(J_3) - i\sqrt{\Delta}}{2} \end{cases} \quad (4)$$

with $\text{tr}(J_2) = m(\ell + 1 - 2m)$; $\Delta = [m(\ell + 1 - 2m)]^2 - 4[m(m - \ell)(1 - m)]$.

Based on the last results, the singularities and the phase portraits of the neighborhood of all equilibriums are summarized in Table 1.

Numerical simulations via matcont software

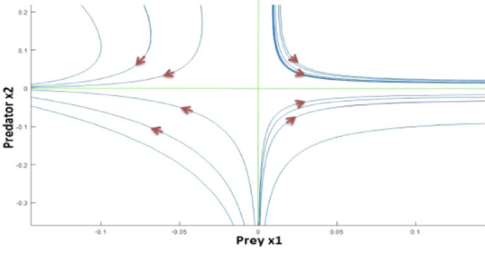
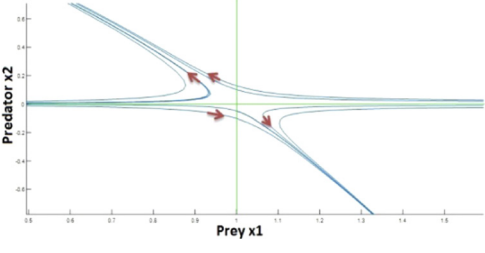
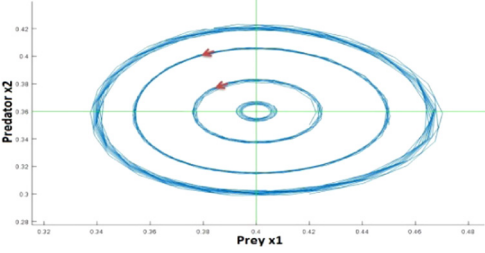
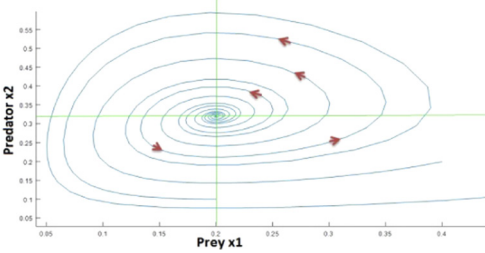
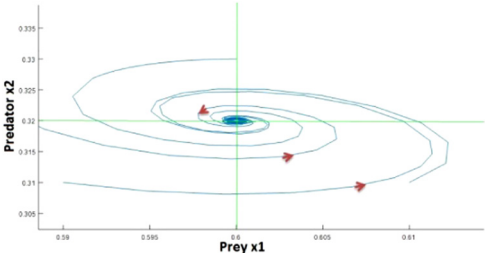
The global dynamics of the system (1), already detailed in Table 1, will be proved numerically in this section using the Matcont software (Dhooge et al., 2008). Since the two first equilibriums E_0 and E_1 exist $\forall m \in [0, 1]$, only the singularity of the equilibrium E_3 will be shown numerically in the following for the initial condition $(x_1 = 0.4; x_2 = 0.3)$. For $m = -\ell = 0.2$, Figure 1 shows the temporal evolution of the dynamics of system (1) whereas the phase portrait of the system is shown in Figure 2.

As it is shown, a heteroclinic orbit appears indicating the existence of a global bifurcation described by an attractor which bifurcates from an unstable focus equilibrium point to a heteroclinic cycle. The two populations' dynamics oscillate between 0 and 1 density values. Figures 3 and 4 show the dynamic behavior of the system at the non-isolated point $E_3 (0.4, 0.36)$ when $m = 0.4$.

For the second case study, the obtained behavior of the two populations is periodic which is described as a circle around the equilibrium $E_3 (0.4, 0.36)$. When $m = 0.6$, the dynamic behavior of the system is shown in Figures 5 and 6.

The obtained phase portrait shows a stable focus. This latter closes to a fixed point with the

Table 1. Predator–prey model analysis.

Equilibrium	Singularities	Phase portraits
$E_0 (0,0)$ $\geq 0, \text{Re}(\lambda_2) \leq 0$	Saddle point	
$E_1 (1,0)$ $\geq 0, \text{Re}(\lambda_2) \leq 0$	Saddle point	
$E_2 (m, (m-\ell)/(1-m))$ $\geq 0, \text{Im}(\lambda_2) \leq 0$	$m=0.4$ Center	$m=0.4 \text{Re}(\lambda_1)=\text{Re}(\lambda_2) = 0$ 
	$m < 0.4$ Unstable focus	$m < 0.4 \text{Re}(\lambda_1)=\text{Re}(\lambda_2) \geq 0$ 
	$m > 0.4$ Stable focus	$m > 0.4 \text{Re}(\lambda_1)=\text{Re}(\lambda_2) \leq 0$ 

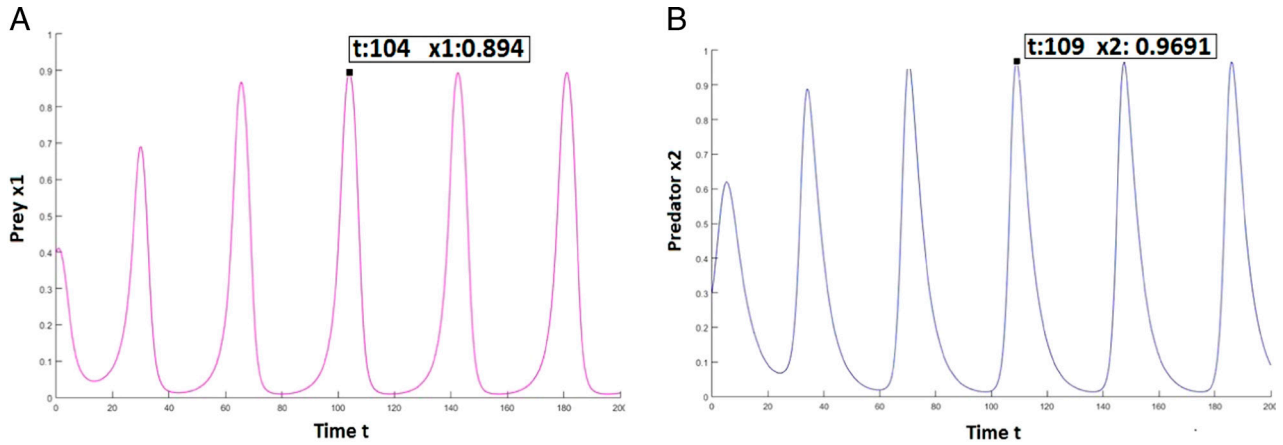


Figure 1: Temporal evolution of the predator-prey system for $m=0.2$: (A) prey and (B) predator.

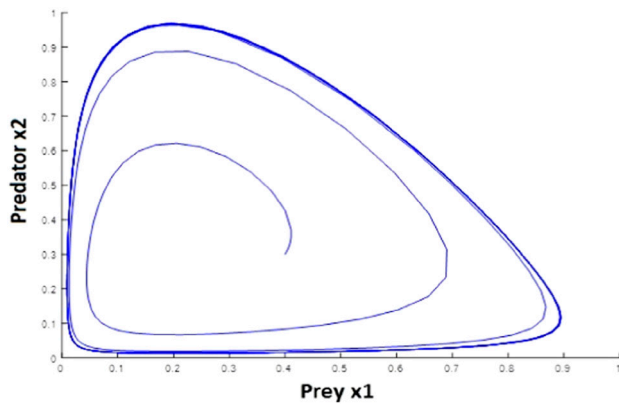


Figure 2: Phase portrait of the predator-prey system for $m=0.2$.

following coordinates (0.6, 0.32) proven with the temporal evolution.

Experimental validation of main nonlinearities

The aim of this section is to design an analog circuit that can build the nonlinear terms according to system (1). Therefore, equivalent electronic circuits of these nonlinear terms are designed and simulated via MultiSIM software (Yujun et al., 2010). Due to the complexity of the equivalent circuit design, we designed first the equivalent circuit of each nonlinear term x^2 and x^3 . The first nonlinear term circuit needs one Multiplier AD6333. The multiplying core of this

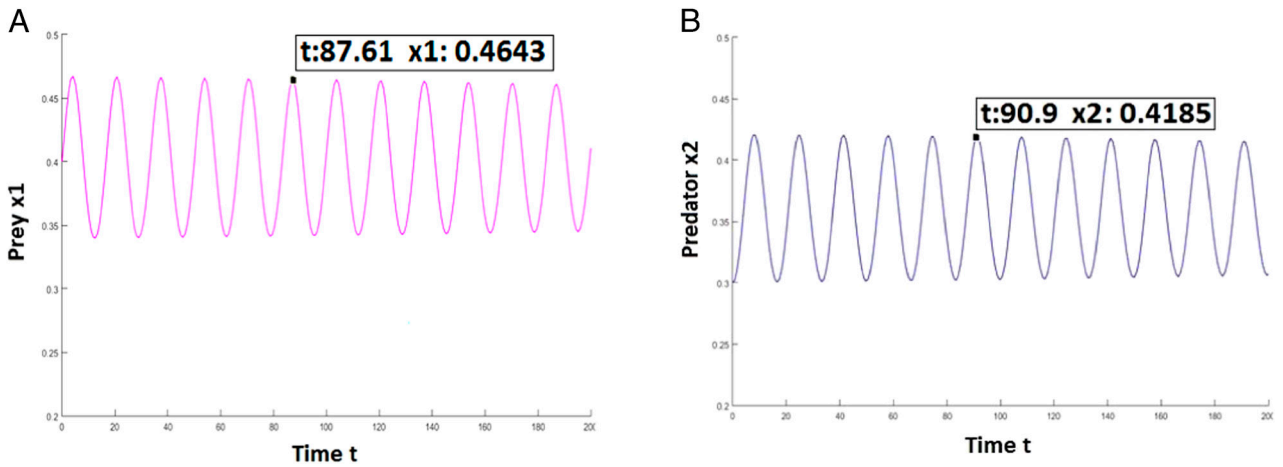


Figure 3: Temporal evolution of the predator-prey system for $m=0.4$: (A) prey and (B) predator.

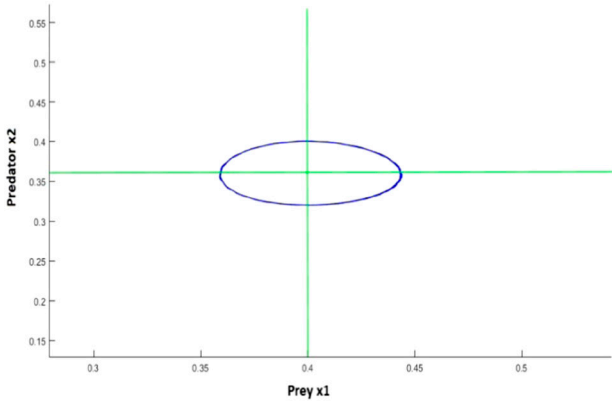


Figure 4: Phase portrait of the predator-prey system for $m = 0.4$.

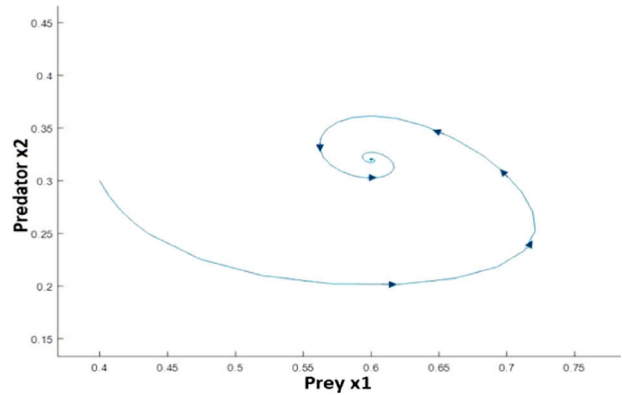


Figure 6: Phase portrait of the predator-prey system for $m = 0.6$.

multiplier comprises a buried Zener reference providing an overall scale factor of 10V. For that, an amplification of the output with a gain of 10 is required. Thus, the equivalent electrical model of x^2 is realized as follows:

$$S_1 = x^2 = \frac{x^2}{10} \frac{(R_1 + R_2)}{R_1}$$

As shown in Figure 7, by considering the components datasheet, the electronic circuit of the nonlinear term x^2 is modeled by one Analog multiplier AD633AN, one Amplifier AOP, two capacitors (C_1, C_2) and two resistors (R_2, R_2). Due to the existence of internal loss in the electrical components, the ideal value of R_2 chosen to obtain the best result is 0.9 kΩ. However, for the nonlinear term x^3 , the electronic circuit is modeled in Figure 8 by two multipliers AD633AN, 2 Amplifiers AOP, four capacitors and four resistors, since its electrical model is realized as follows:

$$S_2 = x^3 = S_1 \frac{(R_3 + R_4)}{R_3} \frac{x}{10} = \left[\frac{x^2}{10} \frac{(R_1 + R_2)}{R_1} \right] \frac{(R_3 + R_4)}{R_3} \frac{x}{10} = \frac{(R_1 + R_2)(R_3 + R_4)}{R_1 R_3} \frac{x^3}{100}$$

The input which will be used for the equivalent circuit of system (1) is continuous. However, in this part, in order to verify the efficiency of the two nonlinear terms equivalent circuits, an alternative signal is used as an input with a weak frequency equal to 1 Hz and amplitude of 2V. The square and the cube of the signal are presented with a pink curve in Figure 9 and Figure 10, respectively. For high frequencies (1 kHz, 10kHz, 100kHz), we obtained the same following results.

As it is shown, we have chosen the same scale for the two nonlinearities. For the first nonlinearity x^2 , the obtained signal amplitude is equal to 4,108V which obviously the square of the input signal amplitude.

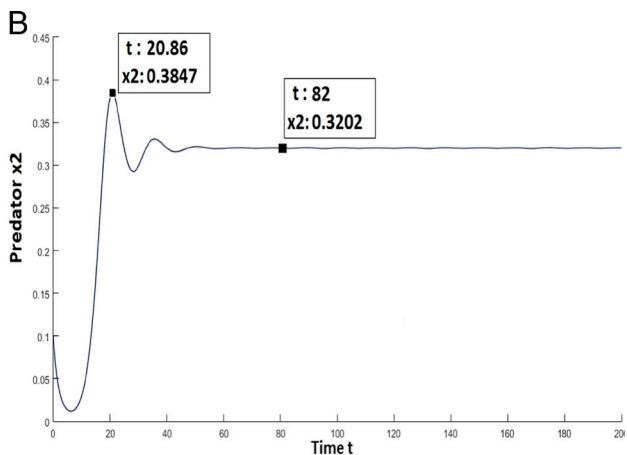
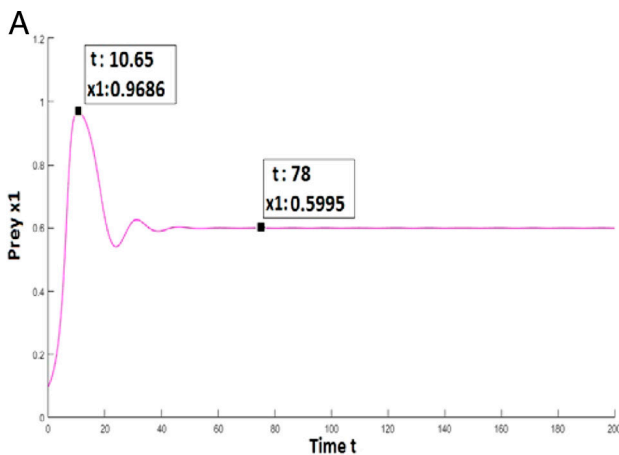


Figure 5: Temporal evolution of the predator-prey system for $m = 0.6$: (A) prey and (B) predator.

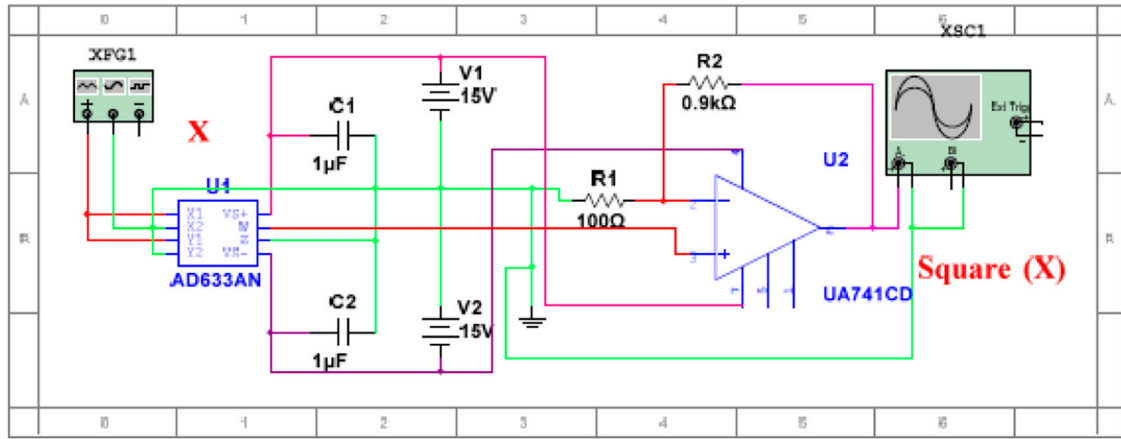


Figure 7: Circuit design of the x^2 function within MultiSIM software.

In addition, for the second nonlinearity x^3 , the result proves that the obtained signal is the cubes of the input signal since the obtained amplitude is equal to 7,980V which is almost equal to 8V the cube of the input amplitude.

Figures 11 and 12 show an experimental implementation for the last simulation results. The oscilloscope traces of the proposed circuit are illustrated in Figures 13 and 14.

Comparing the different results, it is proven that there is a good qualitative agreement between the

numerical simulations with Matlab, the electrical simulations with MultiSIM and the experimental results for the two nonlinearities.

Circuit design via multsim software

In this section, the agreement between biological theory and electronic experiments of the predator-prey model will be analyzed by considering the three cases studies presented numerically by MATCONT. Therefore, a trans-

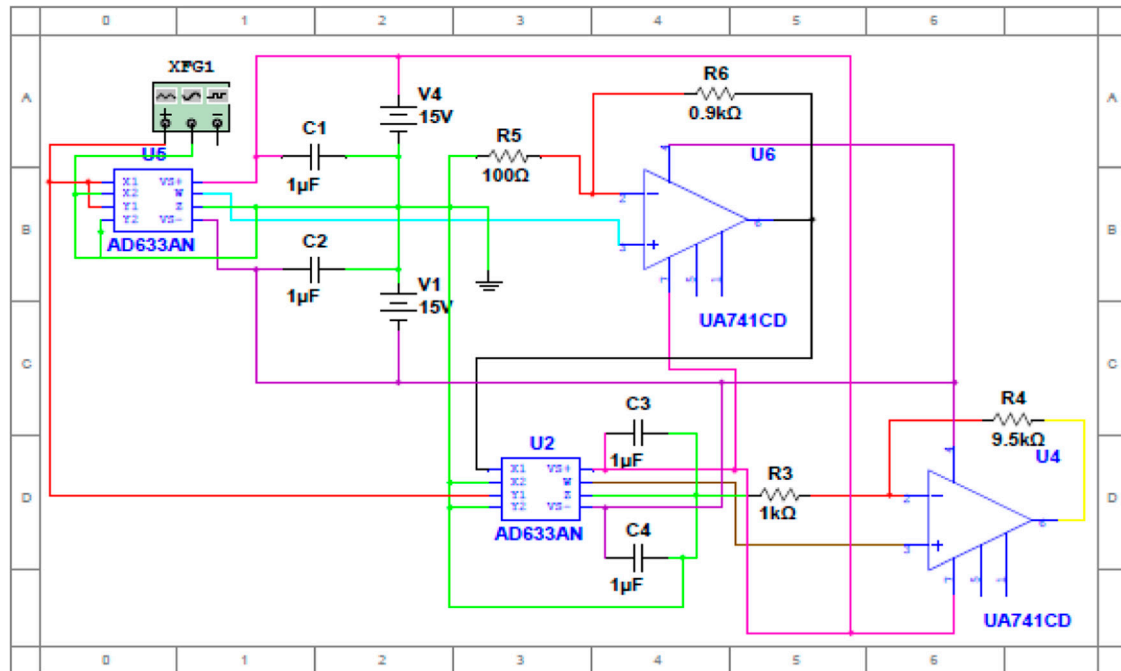


Figure 8: Circuit design of the x^3 function within MultiSIM software.

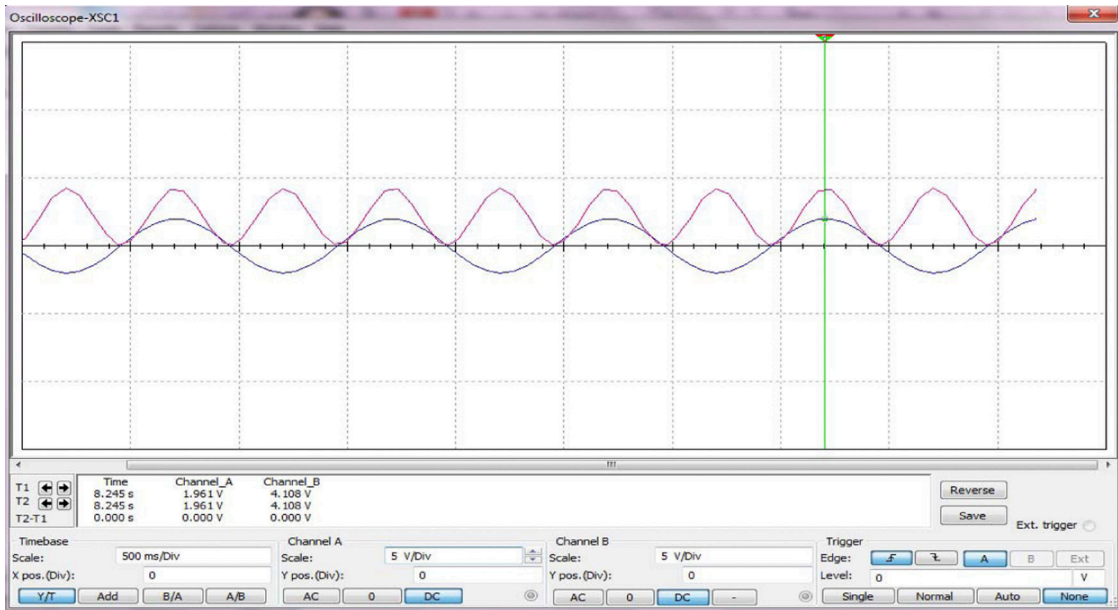


Figure 9: Simulation results of the x^2 function with MultiSIM Software.

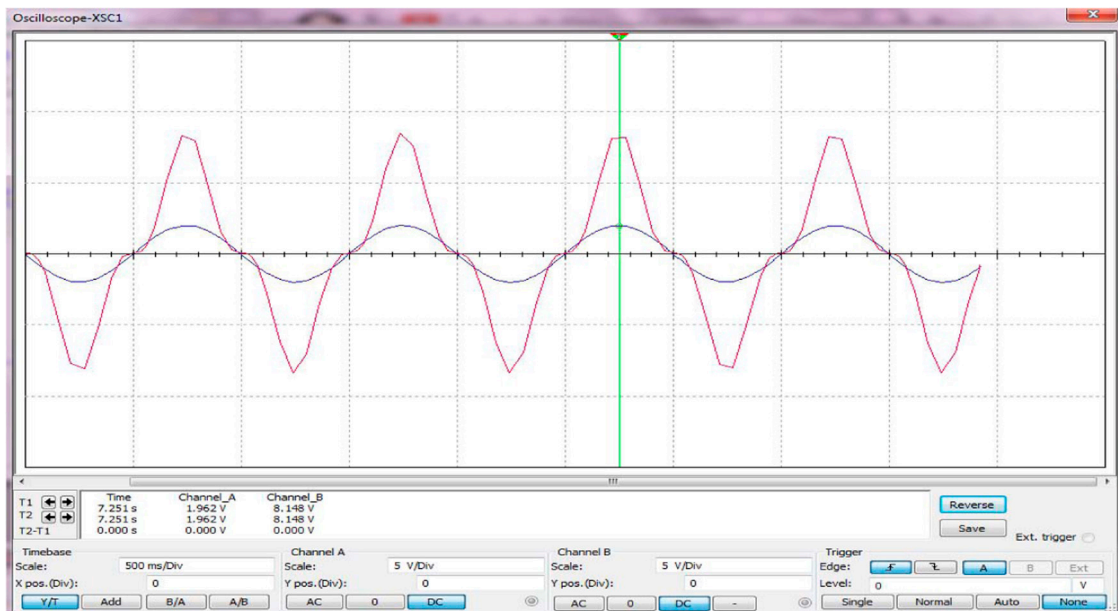


Figure 10: Simulation results of the x^3 function with MultiSIM Software.

formation of the biological predator–prey model (1) to an equivalent electrical model is realized as follows:

$$\begin{cases} \frac{dx_1}{dt} = \frac{1}{C_1 R_1} x_1^3 + \frac{1}{C_1 R_2} x_1^2 - \frac{1}{C_1 R_3} x_1 - \frac{1}{C_1 R_4} x_1 x_2 \\ \frac{dx_2}{dt} = \frac{1}{C_2 R_5} x_1 x_2 - \frac{1}{C_2 R_6} x_2, \end{cases} \quad (5)$$

where $\frac{1}{C_1 R_1} = \frac{1}{C_1 R_4} = \frac{1}{C_2 R_5} = 1, \frac{1}{C_1 R_2} = (1+l); \frac{1}{C_2 R_3} = l,$

$\frac{1}{C_2 R_6} = m$ C_1 and C_2 are used for the integration of the circuit outputs in order to obtain as output the populations' density x_1 and x_2 .

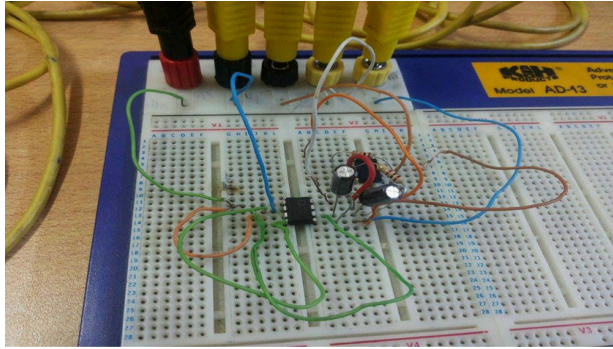


Figure 11: Electronic circuit of the x^2 function.

The electronic circuits corresponding to these cases are designed by the software MultiSIM and presented in the following. We have used three multipliers, five AOP, two capacitors and 12 resistors. The resistors (R_1, R_2, \dots, R_6) and capacitors values are fixed with respect to the parameters values. The value of the two capacitors C_1 and C_2 is fixed at 100nF. In addition, two interrupters $S1$ and $S2$ are used to introduce the initial conditions of the prey and predator density. In order to analyze the three case studies, we vary the value of the resistor R_6 which corresponds to the parameter m since $R_6 = \frac{R_5}{m}$. In the first case study, we consider the mortality rate of the predator $m=0.2$. Therefore, the fixed value of R_6 in this case is equal to 50k Ω . Figure 15 describes the electrical circuit of the predator-prey model (5).

Then, the temporal evolution and the phase portrait when $m=0.2$ are presented in Figure 16 and Figure 17, respectively.

We obtained two phase-shifted alternative signals. The pink curve corresponds to the dynamic evolution of the prey while the blue one corresponds to the dynamic evolution of the predator. Based on the scale chosen in the temporal evolution,

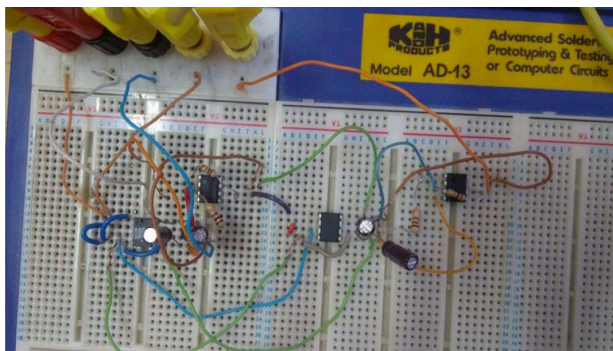


Figure 12: Electronic circuit of the x^3 function.

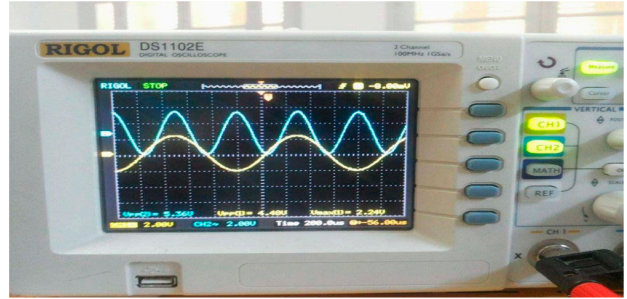


Figure 13: Experimental results of x^2 function.

the amplitude of the blue and pink curves are almost equal to 0.956V and 0.836V, respectively. Comparing with the numerical simulation presented in Figures 1 and 2, we conclude that the permanent regime of the system dynamic obtained via MultiSIM is similar to that obtained using the Matcont software.

In the second case study, we consider the mortality rate of the predator $m=0.4$. Thus, Figure 18 describes the electrical circuit of the model with $R_6=25k\Omega$. Then, the temporal evolution and the phase portrait are illustrated in Figure 19 and Figure 20, respectively.

As it is illustrated in the temporal evolution, the maximum amplitude of the prey population is equal to 0.488V and that of the predator population is equal to 0.441V. The obtained values are obviously very close to the numerical values shown in Figure 3. Furthermore, the phase portrait proves the existence of the center singularity which is demonstrated numerically via the Matcont software in Figure 4.

In the third case study, the mortality rate of the predator m is fixed at 0.6. Therefore, Figure 21

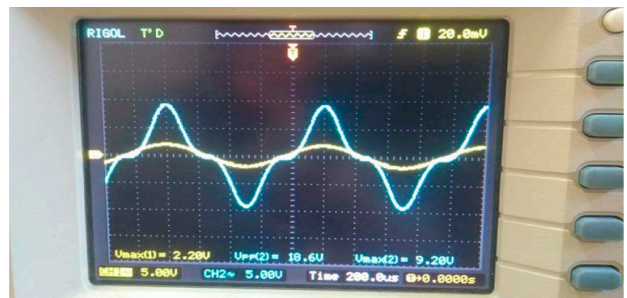


Figure 14: Experimental results of x^3 function.

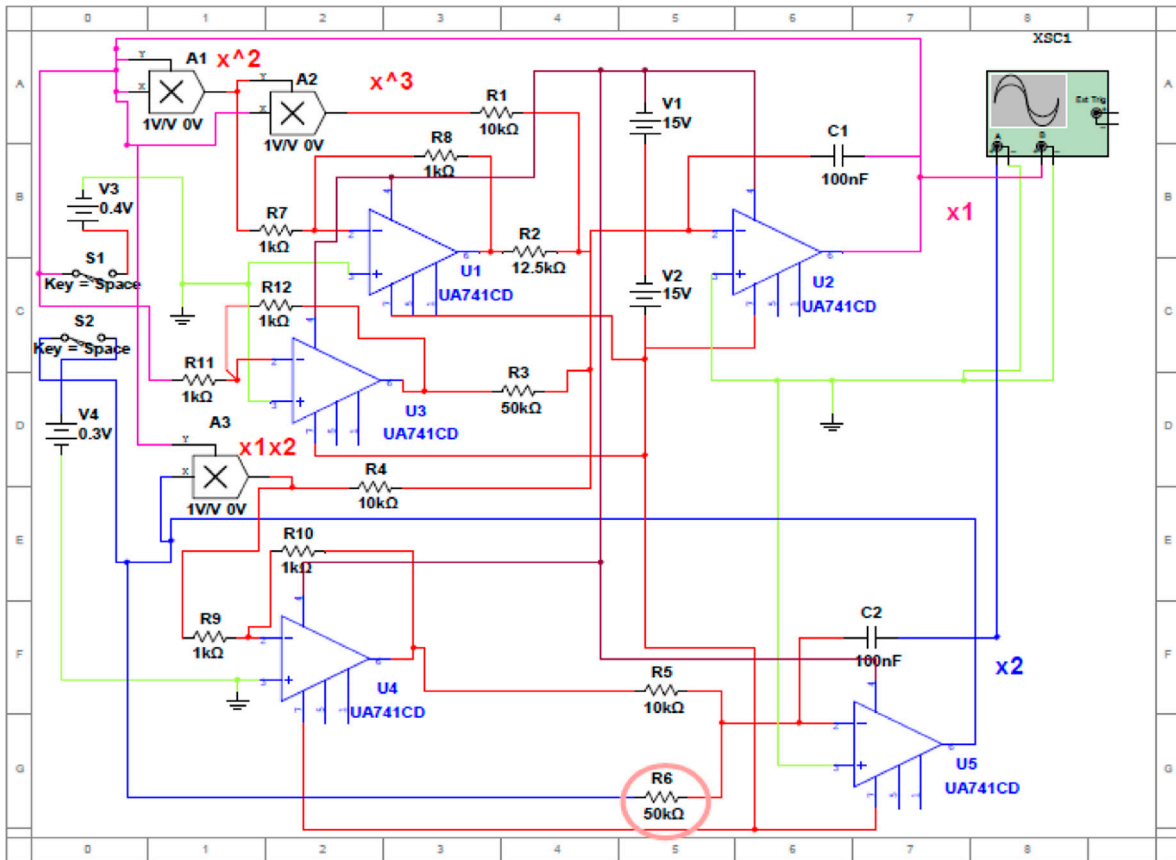


Figure 15: Circuit design of the predator-prey system for $m = 0.2$.

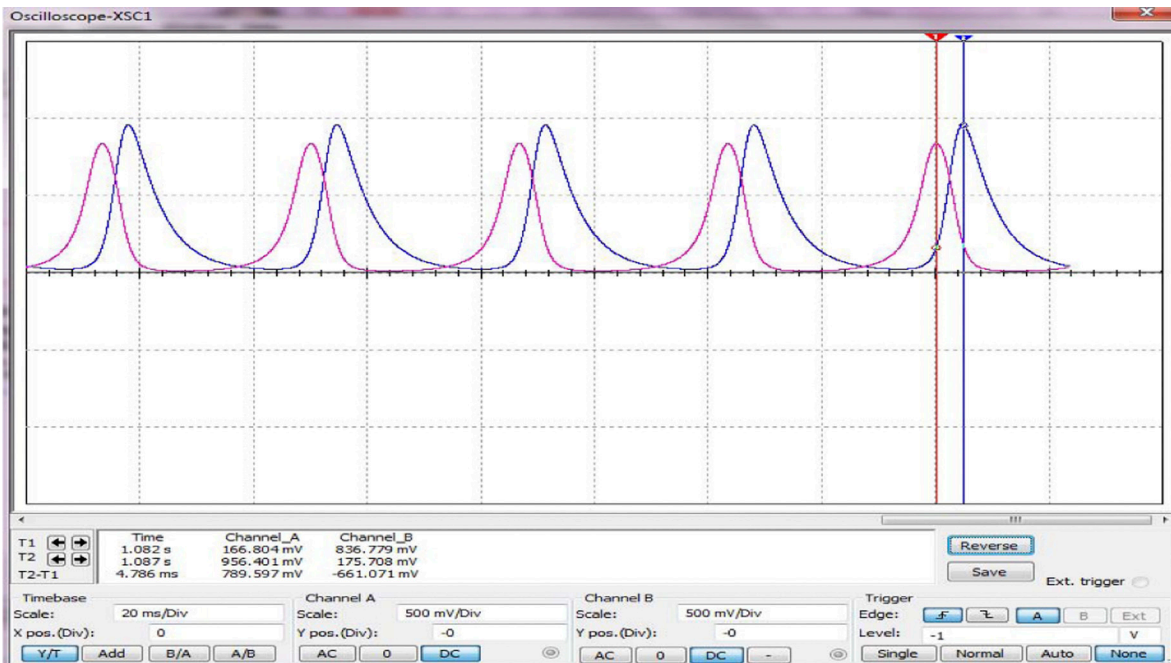


Figure 16: Temporal evolution via MultiSIM software ($m = 0.2$).

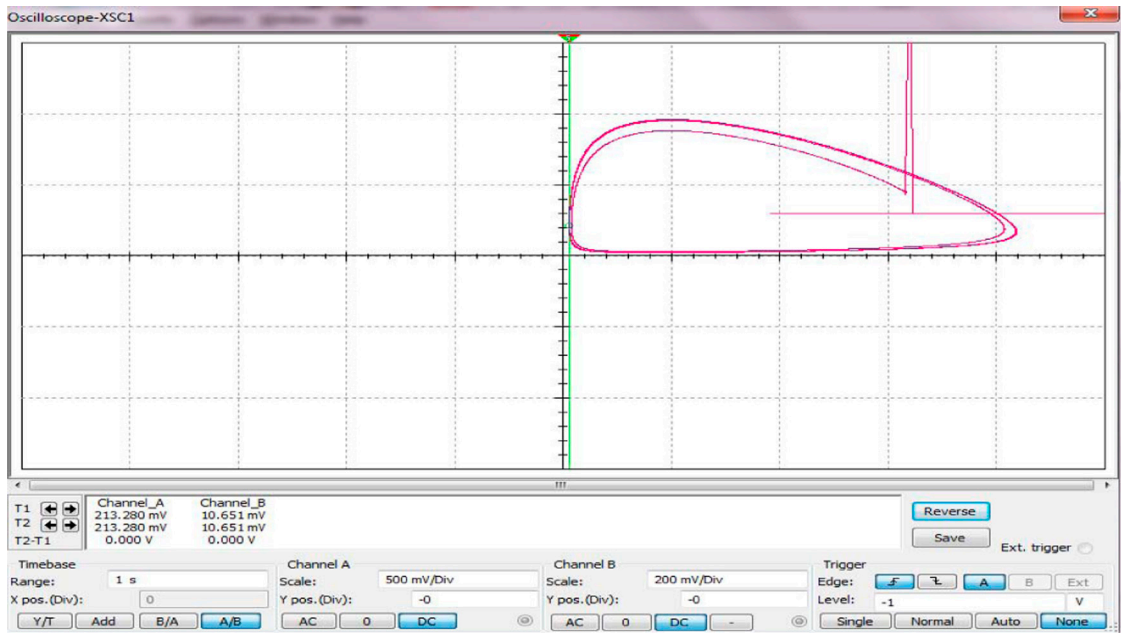


Figure 17: Phase portrait via MultiSIM software ($m = 0.2$).

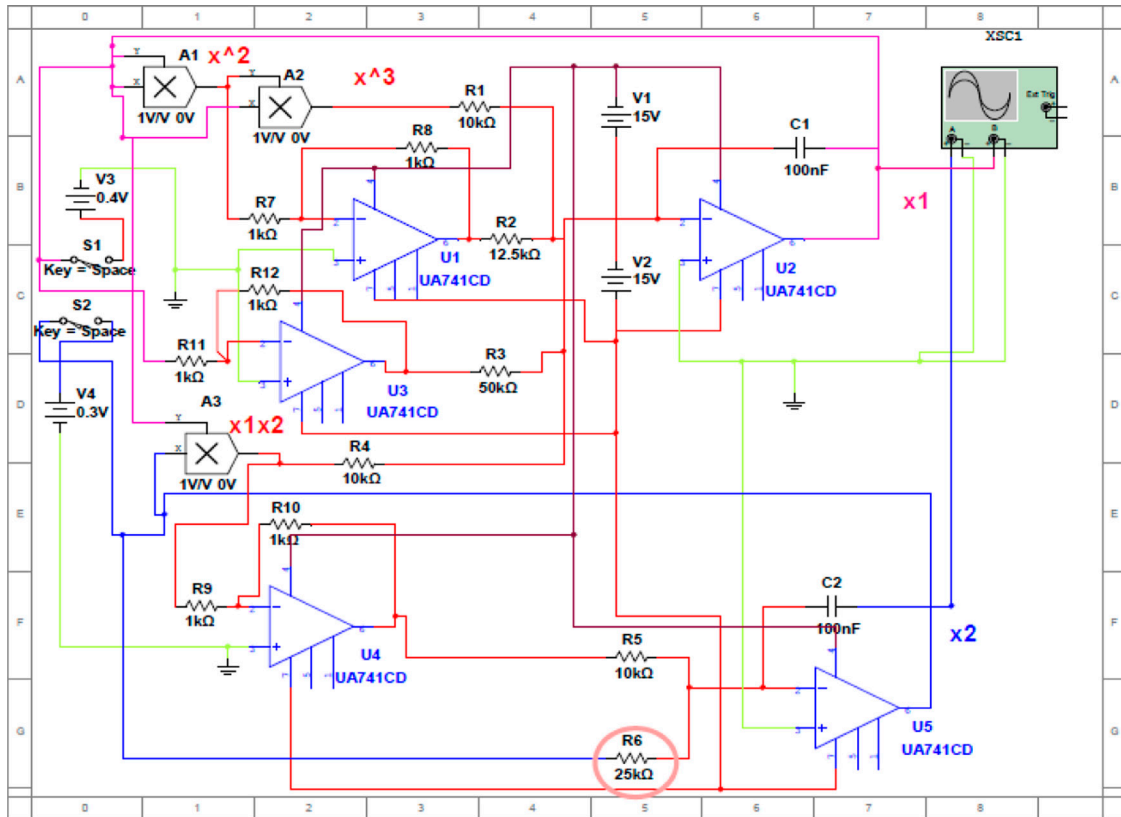


Figure 18: Circuit design of the predator-prey system for $m = 0.4$.

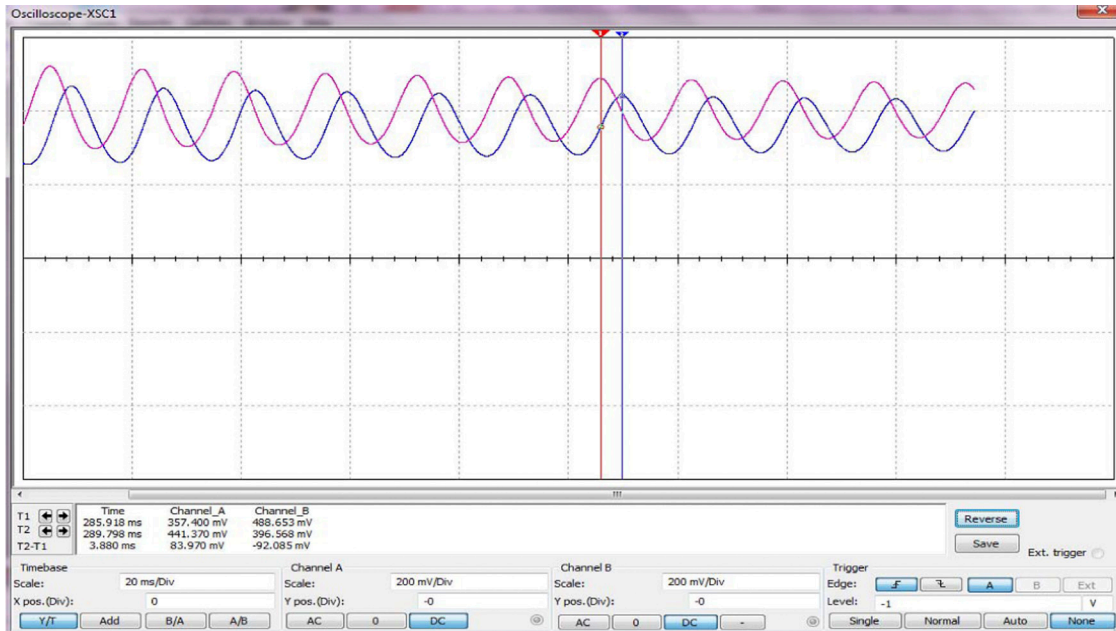


Figure 19: Temporal evolution via MultiSIM software ($m = 0.4$).

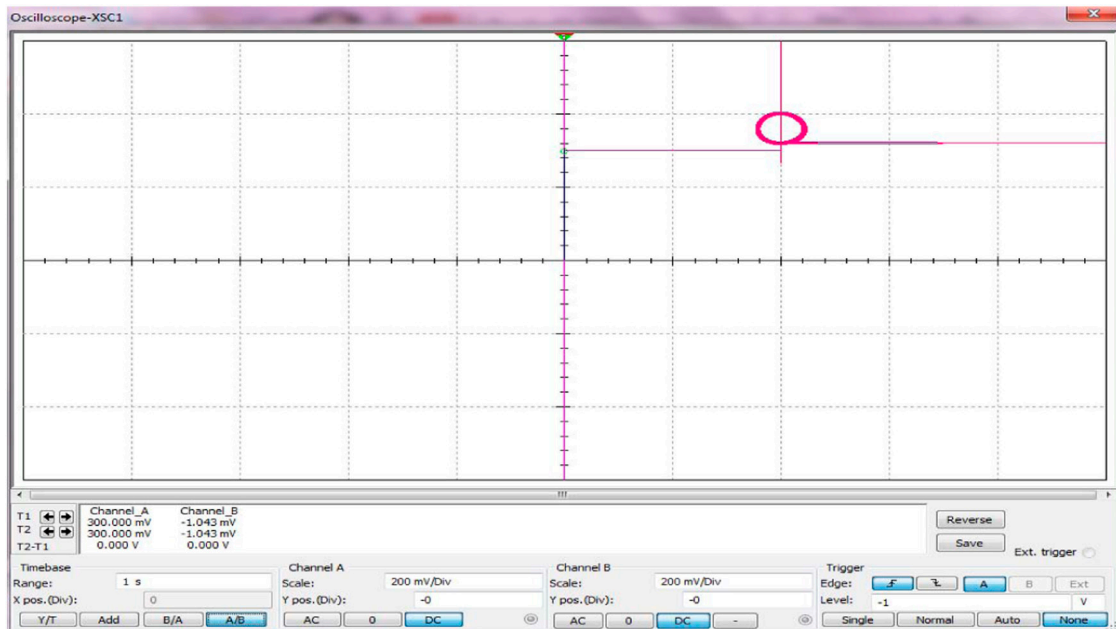


Figure 20: Phase portrait via MultiSIM software ($m = 0.4$).

presents the electrical circuit with $R_6 = 17 \text{ k}\Omega$. Figures 22 and 23 illustrate the corresponding temporal evolution and phase portrait.

For the third case study, we change slightly the initial conditions ($x_1=0.4, x_2=0.1$) to obtain the clearest

results. The obtained temporal evolution and phase portrait prove that the model dynamic tends toward a fixed point. In Figure 22, it is noted that the dynamic behavior oscillates during the transitional regime, whereas in the permanent regime, it becomes

Circuit design and experimental investigations for a predator-prey model

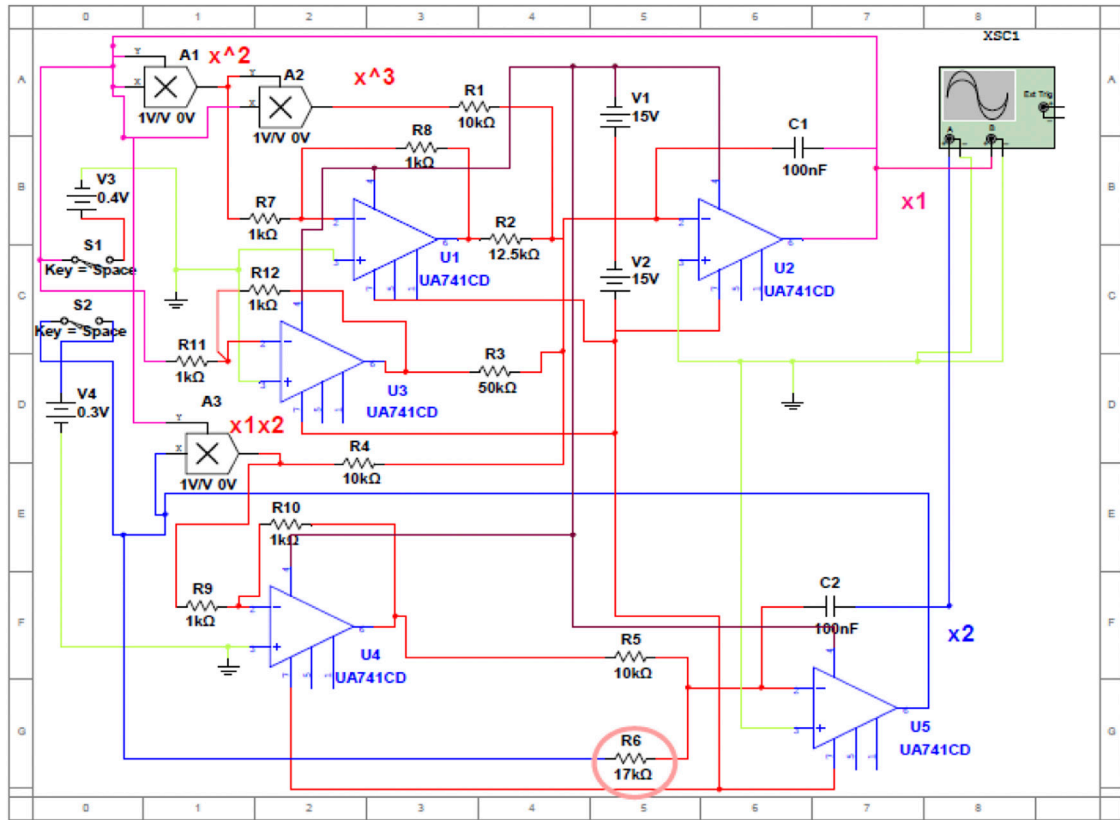


Figure 21: Circuit design of the predator-prey system for $m = 0.6$.

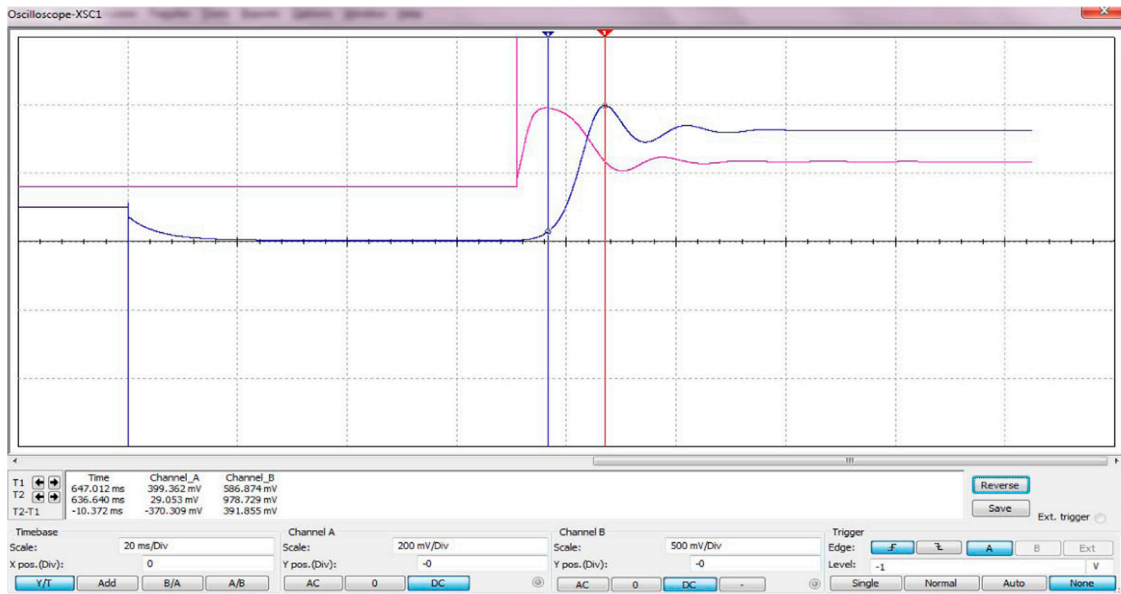


Figure 22: Temporal evolution via MultiSIM software ($m = 0.6$).

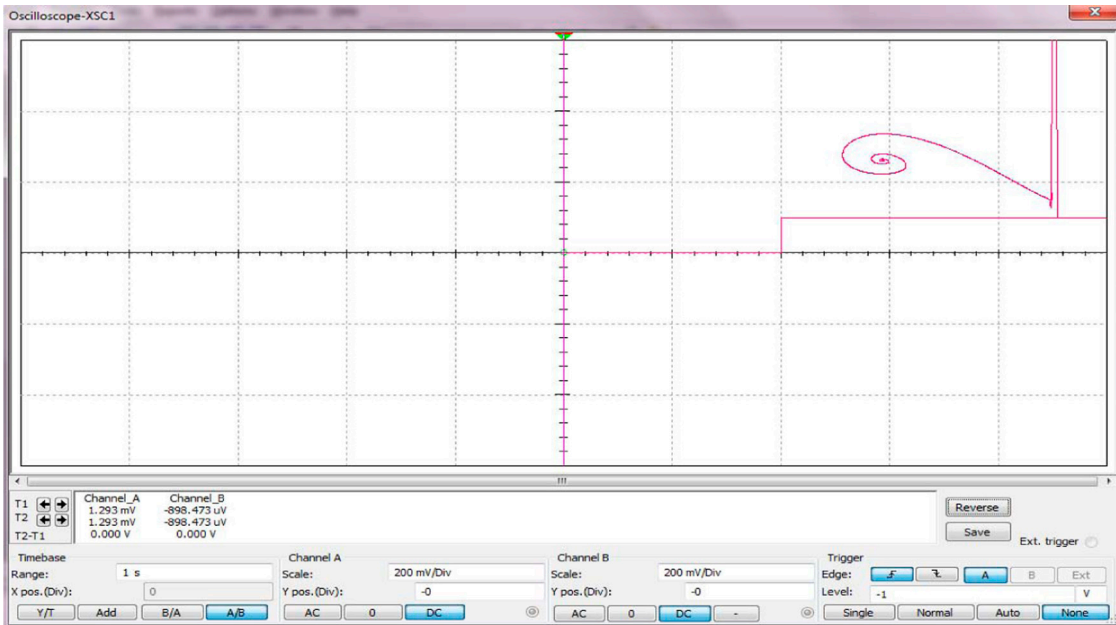


Figure 23: Phase portrait via MultiSIM software ($m=0.6$).

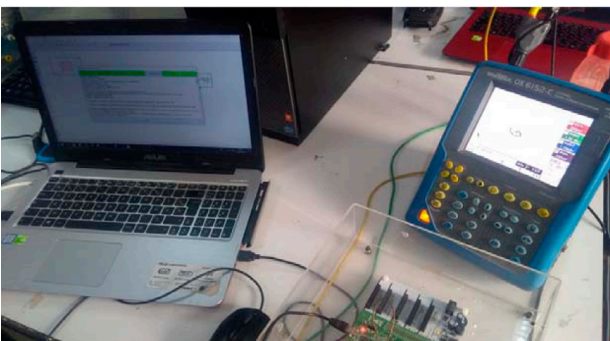
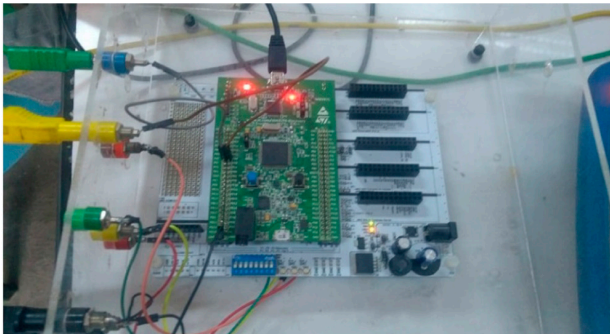


Figure 24: STM3278 Technology.

continuous reaching a constant value equal to 0.586V for the prey population and to 0.326V for the predator one. The pink curve corresponding to the prey population dynamic reaches

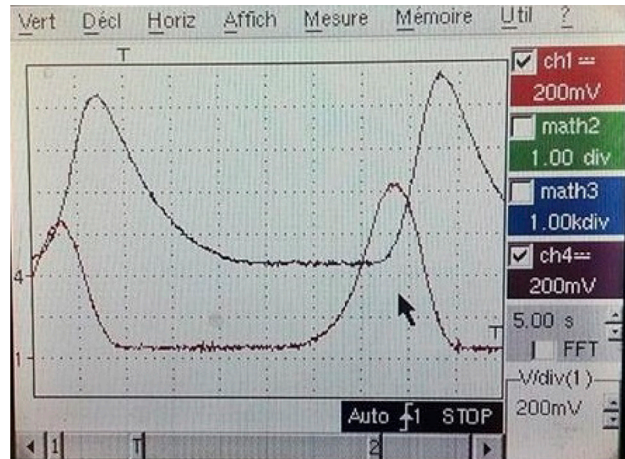


Figure 25: Experimental temporal evolution ($m=0.2$).

a pick of 0.978V. However, the blue curve corresponding to the predator population reaches a pick equal to $x^2=0.399V$. This temporal behavior is described by a stable focus in the obtained phase portrait. These electrical results are almost similar to the numerical ones presented in Figures 5 and 6.

For the three cases study, we conclude that the electrical results obtained by the software MultiSIM obviously prove the numerical results obtained by the Matcont software.

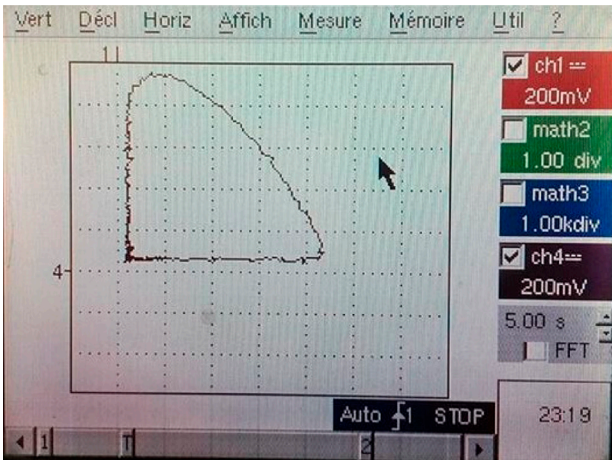


Figure 26: Experimental phase portrait ($m=0.2$).

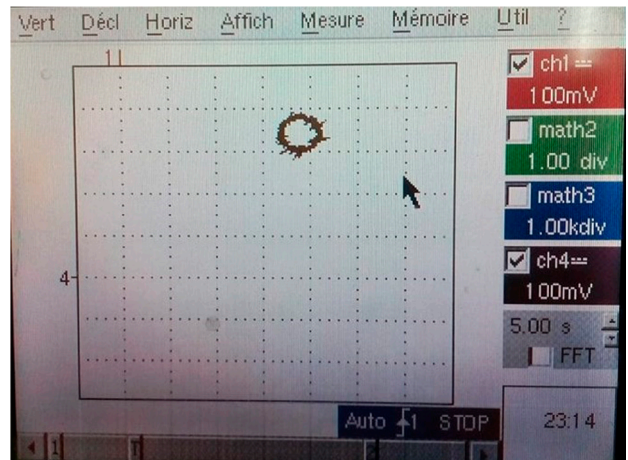


Figure 28: Experimental phase portrait ($m=0.4$).

Experimental implementation of the predator–Prey model

In this section, an experimental implementation of the equivalent electrical circuit will be realized by placing the different electrical components on a bread board within the laboratory.

As it is mentioned previously, mathematical predator–prey model has several nonlinearities which are modeled by multipliers AD633 in the equivalent electrical circuit. The cascade of components AD633 and AOP with gain of 10 amplifies most likely the imperfection and the uncertainties of the electronic components and consequently distorts the experimental results. Therefore, in order to resolve this problem, the experimental validation is realized by using the technology STM3278 shown in Figure 24.

The experimental results of the three cases studied are obtained by using the oscilloscope and presented in Figures 25–30.

Comparing experimental results with numerical results obtained via the MATCONT software shown in Figures 1–6, we can conclude that good agreement is obtained between simulation results and experiments.

Conclusion

In this paper, an electronic circuit is designed for the model of a prey–predator model and its complex behavior is proved via numerical and electrical results. Furthermore, some experimental investigations are also shown and demonstrate that they can be used to characterize the ecological dynamics faster. In the future, we will try to prove, via experimental results,

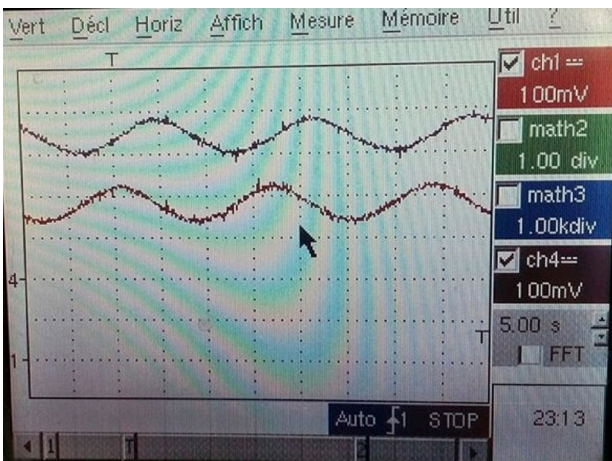


Figure 27: Experimental temporal evolution ($m=0.4$).

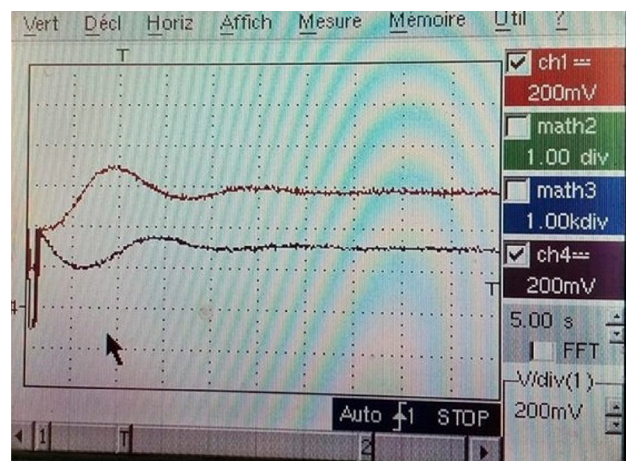


Figure 29: Experimental temporal evolution ($m=0.6$).

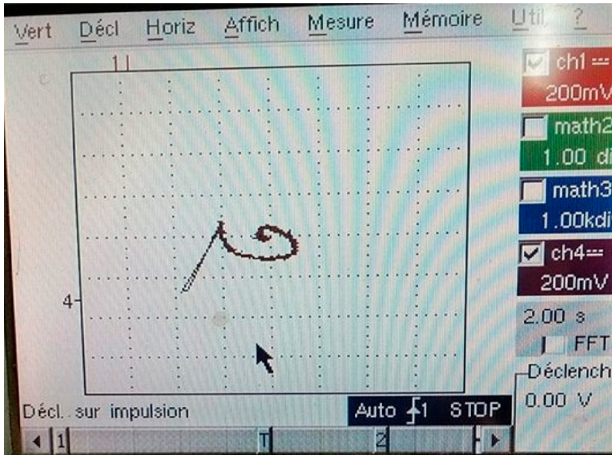


Figure 30: Experimental phase portrait ($m=0.6$).

the chaotic dynamics of such nonlinear systems in the presence of seasonally effects in order to use such circuits for encryption/decryption fields.

Literature Cited

Ben Saad, A., and Boubaker, O. 2015. On bifurcation analysis of the predator-prey BB-model with weak allee effect. *IEEE 16th international conference on Sciences and Techniques of Automatic Control and Computer Engineering*, Monastir, 19–23.

BenSaad, A., and Boubaker, O. 2017. A new fractional-order predator-prey system with allee effect, in Azar, A.T., Vaidyanathan, S., and Ouannas, A. (eds), *Fractional Order Control and Synchronization of Chaotic Systems* 688, Springer, Berlin, 857–77.

Bürger, R., Ruiz-Baier, R., and Tian, C. 2017. Stability analysis and finite volume element discretization for delay-driven spatio-temporal patterns in a predator-prey model. *Mathematics and Computers in Simulation* 132: 28–52.

Dhooge, A., Govaerts, W., Kuznetsov, Y.A., Meijer, H.G.E., and Sautois, B. 2008. New features of the software MatCont for bifurcation analysis of dynamical systems. *Mathematical and Computer Modelling of Dynamical System* 14: 147–75.

Elettrey, M.F., Al-Raezah, A.A., and Nabil, T. 2017. Fractional-Order Model of Two-Prey one-predator system. *Mathematical Problems in Engineering* 2017.

Feng, X., Shi, K., Tian, J., and Zhang, T. 2017. Existence, multiplicity, and stability of positive solutions of a predator-prey model with dinosaur functional response. *Mathematical Problems in Engineering* 2017.

Gómez, F., Bernal, J., Rosales, J., and Cordova, T. 2012. Modeling and simulation of equivalent circuits in description of biological systems—a fractional calculus approach. *Journal of Electrical Bioimpedance* 3: 2–11.

Kengne, J., Jafari, S., Njitacke, Z.T., Khanian, M.Y.A., and Cheukem, A. 2017. Dynamic analysis and electronic circuit implementation of a novel 3D autonomous system without linear terms. *Communications in Nonlinear Science and Numerical Simulation* 52: 62–76.

Laktionov, I.S., Vovna, O.V., and Zori, A.A. 2017. Planning of remote experimental research on effects of greenhouse microclimate parameters on vegetable crop-producing. *International Journal on Smart Sensing and Intelligent Systems* 10(4): 845–62.

Lassoued, A., and Boubaker, O. 2016. On new chaotic and hyperchaotic systems: a literature survey. *Nonlinear Analysis: Modelling and Control* 21(6): 770–89.

Lassoued, A., and Boubaker, O. 2017. Dynamic analysis and circuit design of a novel hyperchaotic system with fractional-order terms. *Complexity* 2017.

Le Masson, S., Laflaquerie, A., Bal, T., and Le Masson, G. 1999. Analog circuits for modeling biological neural networks: design and applications. *IEEE Transactions on Biomedical Engineering* 46(6).

Li, H.L., Zhang, L., Hu, C., Jiang, Y.L., and Teng, Z. 2017b. Dynamical analysis of a fractional-order predator-prey model incorporating a prey refuge. *Journal of Applied Mathematics and Computing* 54(1–2): 435–49.

Li, M., Chen, B., and Ye, H. 2017a. A bioeconomic differential algebraic predator-prey model with nonlinear prey harvesting. *Applied Mathematical Modelling* 42: 17–28.

Liu, G., Wang, X., Meng, X., and Gao, S. 2017. Extinction and persistence in mean of a novel delay impulsive stochastic infected predator-prey system with jumps. *Complexity* 2017.

Liu, M., He, X., and Yu, J. 2018. Dynamics of a stochastic regime-switching predator-prey model with harvesting and distributed delays. *Nonlinear Analysis: Hybrid Systems* 28: 87–104.

Liu, W., and Wiang, Y. 2018. Bifurcation of a delayed gause predator-prey model with michaelis-menten type harvesting. *Journal of Theoretical Biology* 438: 116–32.

Liu, X., and Dai, B., Dynamics of a predator-prey model with double allee effects and impulse. *Nonlinear Dynamics* 88(1): 685–701.

Luo, Z., Lin, Y., and Dai, Y. 2016. Rank one chaos in periodically kicked lotka-volterra predator-prey system with time delay. *Nonlinear Dynamics* 85: 797–811.

- Mehdi, H., and Boubaker, O. 2011. Position/force control optimized by particle swarm intelligence for constrained robotic manipulators. In IEEE 11th International Conference on Intelligent Systems Design and Applications (ISDA), Nov. 22–24, 2011, Cordoba, Spain, 190–195.
- Mehdi, H., and Boubaker, O. 2016. PSO-Lyapunov motion/force control of robot arms with model uncertainties. *Robotica* 34(3): 634–51.
- Pang, S., Zhang, W., Ma, T., and Gao, Q. 2017. Ant colony optimization algorithm to dynamic energy management in cloud data center. *Mathematical Problems in Engineering* 2017.
- Sidhu, D.S., and Dhillon, J.S. 2017. Design of digital IIR filter with conflicting objectives using hybrid predator–prey optimization. *Circuits, Systems, and Signal Processing*, 1–25.
- Teay, S.H., Batunlu, C., and Albarbar, A. 2017. Smart sensing system for enhancing the reliability of power electronic devices used in wind turbines. *International Journal on Smart Sensing and Intelligent Systems* 10(2): 407–24.
- Umar, L., Setiadi, R.N., Hamzah, Y., and Linda, T.M. 2017. An Arduino Uno based biosensor for water pollution monitoring using immobilized Algae *Chlorella Vilgaris*. *International Journal on Smart Sensing and Intelligent Systems* 10(4) 955–75.
- Visconti, P., Primiceri, P., de Fazio, R., and Ekuakille, A.L. 2017. A solar-powered white led-based UV-VIS spectrophotometric system managed by PC for air pollution detection in faraway and unfriendly locations. *International Journal on Smart Sensing and Intelligent Systems* 10(1): 18–49.
- Volterra, V. 1928. Variations and fluctuations of the number of individuals in animal species living together. *ICES Journal of Marine Science* 3(12): 3–51.
- Yongwang, L., Yu-ming, L., Heng-bin, Q., and Yan-feng, B. 2017. A new mathematical method for solving cuttings transport problem of horizontal wells: ant colony algorithm. *Mathematical Problems in Engineering* 2017.
- Yuan, H., Wu, J., Jia, Y., and Nie, H. 2018. Coexistence states of a predator–prey model with cross-diffusion. *Nonlinear Analysis: Real World Applications* 41: 179–203.
- Yujun, N., Xingyuan, W., Mingjun, W., and Huaguang, Z. 2010. A new hyperchaotic system and its circuit implementation. *Communication in Nonlinear Science and Numerical Simulation* 15: 3518–24.
- Zhang, B., and Duan, H. 2017. Three-dimensional path planning for uninhabited combat aerial vehicle based on predator–prey pigeon-inspired optimization in dynamic environment. *IEEE/ACM Transactions on Computational Biology and Bioinformatics (TCBB)* 14(1): 97–107.
- Zhang, L., Liu, J., and Banerjee, M. 2017a. Hopf and Steady state bifurcation analysis in a ratio-dependent predator–prey model. *Communications in Nonlinear Science and Numerical Simulation* 44: 52–73.
- Zhang, X., Li, Y., and Jiang, D. 2017b. Dynamics of a stochastic holling type II predator–prey model with hyperbolic mortality. *Nonlinear Dynamics* 87(3): 2011–20.